J Porous Mater (2016) 23:539–547
DOI 10.1007/s10934-015-0107-6

The role of $CuO–TiO_2$ additives in the preparation of high-strength porous alumina scaffolds using directional freeze casting

Yujie Fu[1] · Ping Shen[1] · Zhijie Hu[1] · Chang Sun[1] · Ruifen Guo[1] · Qichuan Jiang[1]

Published online: 17 December 2015

Abstract Lamellar porous Al_2O_3 scaffolds with initial solid loading of 30 vol% were prepared by freeze casting using micron-sized Al_2O_3 powders as raw material and $CuO–TiO_2$ additives as sintering aid. The effects of the composition of $CuO–TiO_2$ on the microstructure, porosity and compressive property of the Al_2O_3 scaffolds were investigated and the mechanisms for sintering promotion addressed. The sintering aid effect was prominent when $CuO:TiO_2$ was 1:2 in mass and their amount reached 3 wt% of the total ceramic powders. The corresponding compressive strength reached 176 ± 20 MPa with the porosity being 45 ± 1 % after sintering at 1450 °C for 2 h. Activation of the Al_2O_3 lattice due to partial substitution of Ti^{4+} for Al^{3+} and formation of a low-melting eutectic liquid were presumed to play a significant role in the sintering and strengthening of the Al_2O_3 scaffolds.

Keywords Freeze casting · Porous ceramics · Sintering aids · Compressive strength

1 Introduction

Porous ceramics are widely used as filters, catalyst supports and biomaterials owing to their distinct advantages such as good permeability, high stability and large specific surface area. They can be fabricated by various methods, among which directional freeze casting is attractive due to its simpleness, low cost, environmental friendliness, and great flexibility in producing complex-shaped scaffolds with controlled pore sizes, shapes and orientations in a reliable and economical way. Moreover, the resultant preforms with aligned pores are usually stronger than the products containing similar porosity but with random pores. Therefore, this technique finds wide applications for producing load-bearing biomaterials such as bone substitute and materials for chemical processes and energy sources including SOFC, electrodes, absorbent, sensors, catalysts supports, filtration/separation devices, and photocatalysis for air or water purification [1–4].

A variety of porous materials such as hydroxyapatite [1], alumina [5–14], zirconia [15], silicon carbide [16], nitride [17] and titanium dioxide [18] have been prepared by directional freeze casting. Table 1 summarizes recent progress in the preparation of the porous Al_2O_3 and its composite scaffolds using this technique. The compressive strength of the resultant products is usually higher than that prepared by other methods for the scaffolds with the same porosity mainly because of directional lamellar structures [2]. In practice, in order to produce the scaffolds with high compressive strength, fine Al_2O_3 particles (200–700 nm) and high sintering temperatures (1500–1700 °C) together with long holding times (2–4 h) are usually employed (Table 1), which not only increases production cost but also decreases porosity considerably. Using micron-sized alumina powders is economic; however, the strength of the sintered scaffolds is low. An effective solution could be the addition of appropriate sintering aids in the ceramic slurry, as they can greatly promote the sinterability of the preform at relatively low sintering temperatures. Nevertheless, so far this idea has been seldom adopted in the preparation of freeze-cast Al_2O_3 scaffolds.

✉ Ping Shen
shenping@jlu.edu.cn

[1] Key Laboratory of Automobile Materials (Ministry of Education), Department of Materials Science and Engineering, Jilin University, No. 5988 Renmin Street, Changchun 130025, People's Republic of China

Table 1 Research on porous Al_2O_3 and its composite scaffolds fabricated by directional freeze casting

Materials	Purity (%)/particle size (μm)	Solid loading (vol%)	Sintering temperature (°C)/time (h)	Compressive strength (MPa)	References
Al_2O_3-mullite	–	50[a]	1500/–	90.80 ± 3.70	Heon et al. [5]
Al_2O_3	99.99/0.4	20	1550/2	73.70 ± 5.60	Han et al. [6]
Al_2O_3	–/0.3	25	1600/3	95.00	Yoon et al. [7]
Al_2O_3	99.50/5.0	30	1550/2	64.00 ± 2.00	Shen et al. [8]
Al_2O_3 (20 vol%)–HA	99.99/0.4	20	1550/4	116.60 ± 2.30	Hu et al. [9]
Al_2O_3 (20 wt%)–ZrO_2	–/0.7, 0.1	30	1550/2	81.00 ± 3.00	Liu et al. [10]
Al_2O_3	99.80/0.5	30	1550/3	22.00	Zhang et al. [11]
Al_2O_3	–/1.0	30	1700/2	45.00	Tang et al. [12]
Al_2O_3	99.80/0.5	10	1500/2	18.20	Zeng et al. [13]
Al_2O_3	–/0.2	25	1500/–	153.00 ± 30.00	Chen et al. [14]

[a] Mass fraction

It has been a long history in searching for effective agents for sintering of alumina. Early in 1954, Smothers et al. [19] did a lot of work on low-temperature sintering of Al_2O_3 and indicated that the oxides of Ti, Nb, Mn, Cu and Ge could promote the sinterability. The compacts containing TiO_2, Ti_2O_3 and Nb_2O_5 had obvious dimensional shrinkage after sintering at a temperature as low as 1300 °C for 2 h. In 1995, Horn et al. [20] found that the compacts containing TiO_2 reached a relative density of larger than 99 % after sintering at 1300–1550 °C and the morphology of Al_2O_3 grains changed considerably with the increase in the TiO_2 amount and sintering temperature. Li [21] compared the effect of several oxides, such as MgO, Y_2O_3 and CuO, on the sinterability of Al_2O_3 and concluded that CuO had a noticeable effect at a temperature as low as 1250 °C. More strikingly, Sathiyakumar et al. [22] added 2 mol% CuO and 2 mol% TiO_2 to the Al_2O_3 powders and achieved a density of 99.6 % after sintering at 1200 °C. It should be mentioned that all the aforementioned studies aimed at achieving fully dense Al_2O_3 compacts consisting of uniformly-distributed powders, which is very different from that in the freeze-casting work, whose purpose is to produce porous scaffolds with high strength.

In this work, we prepared the high-strength porous Al_2O_3 scaffolds by using micron-sized alumina powders with the addition of CuO–TiO_2 sintering aids and then low-temperature firing the freeze-cast preforms. We further investigated the effects of the CuO–TiO_2 sintering aids on the sinterability, microstructure and compressive property of the porous products with primary purposes to find out the optimum composition of the CuO–TiO_2 additives and to clarify the sintering mechanism. We hope that this study may provide a simple, versatile and economical way to produce high-strength ceramic scaffolds with controlled porosity and pore structures.

2 Experimental procedure

Commercially available powders of α-Al_2O_3, CuO and TiO_2 with average particle sizes of 5 μm, 3 μm and 30 nm and purities of 99.5, 99.0 and 99.9 %, respectively, were used as raw materials. Sodium polymethacrylate and deionized water were used as dispersant and freezing medium.

First, alumina slurries were prepared by mixing Al_2O_3 powders in an initial solid loading of 30 vol%, CuO–TiO_2 additives in weight percents of 1, 3 and 5 wt% of the total ceramic powders and a small amount (1 wt%) of dispersant (Sodium polymethacrylate) with deionized water. The slurries were ball-milled for 12 h using alumina balls, and then de-aired by stirring in a vacuum desiccator for 20 min to remove the air bubbles. Subsequently, the slurries were poured into polyethylene molds with an inner diameter of 18 mm, whose bottom was placed on a Cu bar and top exposed to air. The Cu bar was inserted in liquid nitrogen and its top surface kept at −20 °C by using a ring heater. Therefore, directional solidification of the slurry from bottom to top was induced. The freeze casting device was similar to that described by Wegst et al. [23].

After frozen, the samples with dimensions of 18 mm in diameter and 30 mm in height were demoulded and transferred to a freeze dryer to sublimate the ice at −50 °C under a vacuum of 10 Pa for 48 h. The dried preforms were heated in air at 4 °C/min to 500 °C, holding for 30 min in order to burn out the organic additive, and then continued to heat at a constant rate of 5 °C/min to a predetermined sintering temperature, holding for 2 h. Finally, they were cooled at 5 °C/min to room temperature.

The shrinkage and porosity of the sintered scaffolds were calculated by measuring the dimensions and mass of the scaffolds before and after sintering. The microstructures of the samples were observed under a scanning electron microscope (Evo 18, Carl Zeiss, Germany) and a field-emission scanning electron microscope (FESEM, JSM-6700F, Japan). The phases were examined by using an X-ray diffractometer (XRD) with Cu-Kα radiation (D/Max 2500PC Rigaku, Japan). The compressive strength of the scaffolds was measured by using a universal testing machine (Instron 5689, Instron Corp., USA) at a crosshead speed of 0.5 mm/s.

3 Results

3.1 Linear shrinkage and porosity

Figure 1 shows the linear shrinkage and porosity of the scaffolds sintered at 1100–1500 °C for 2 h with a 100 °C interval. The addition amount of sintering aids was 3 wt% but the ratio of m(CuO):m(TiO_2) (hereinafter abbreviated as C/T) was different. As indicated in Fig. 1a, the scaffolds with CuO additive showed a noticeable shrinkage only at temperatures higher than 1400 °C. Regarding that the melting point of CuO is only about 1200 °C, this result indicates that the formation of liquid CuO does not seem to make a significant contribution to the densification of Al_2O_3. Instead, the sinterability was greatly improved by the addition of TiO_2. The most prominent effect corresponds to the CuO–TiO_2 composite additives in a mass ratio of 1:2 at relatively low sintering temperatures of less than 1450 °C. The linear shrinkage was noticeable, yet the porosity in the scaffolds was still higher (Fig. 1b). In comparison, the effect of 3 wt% TiO_2 was also significant, particularly at temperatures higher than 1450 °C, but the porosity in the scaffolds dramatically reduced.

Figure 2 shows the variations in linear shrinkage and porosity with sintering temperature for the scaffolds containing different amounts of CuO–TiO_2 at a fixed ratio (C/T = 1:2). In general, with the increase in the addition amount and sintering temperature, the shrinkage of the scaffolds increased as expected and the porosity decreased. However, when the amount of sintering aids reached to 5 wt%, some cracks appeared in the scaffolds sintered at temperatures higher than 1350 °C, as indicated in Fig. 3.

3.2 Microstructures

Figure 4 shows the typical microstructures of the porous Al_2O_3 scaffolds in longitudinal and transverse sections. The lamellar structure is clear and shows a gradient change with the increase in the distance from the bottom surface. The larger the distance, the coarser the lamellae and the wider the lamellar spacing. Such a pattern depends on ice growth morphology during freeze casting. With the increase in the distance away from the cold copper bar, the ice growing velocity at the front decreased progressively due to the poor thermal conductivity of ice and Al_2O_3 powders, leading to increase in the lamellar spacing.

Figure 5 shows the SEM micrographs in the longitudinal section of the scaffolds with 3 wt% sintering aids of different C/T ratios after sintering at 1300 °C for 2 h. They were all taken from the regions about 20 mm above the bottom surface. It is clearly indicated that the lamellar spacing became smaller as the ceramic wall became thinner with the increase in relative amount of TiO_2 in the sintering aids. The Al_2O_3 particles in the scaffold with single CuO additive were relatively fine and separately stacked, as given in the inserted figure in Fig. 5a. For the CuO–TiO_2 composite additive, the Al_2O_3 particles had some abnormal growth and the porosity

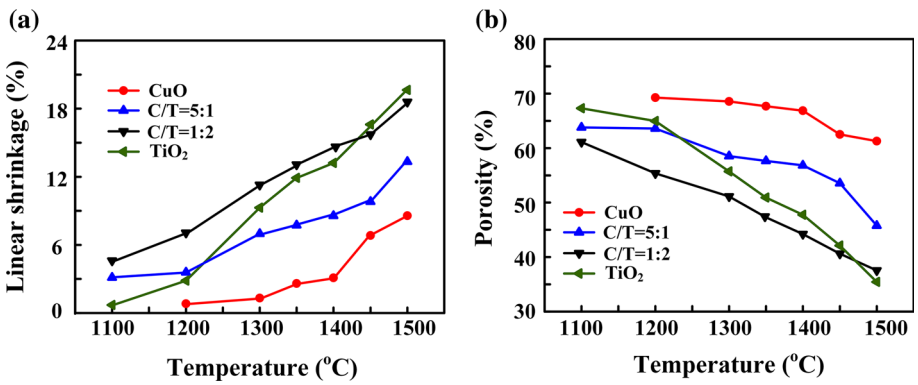

Fig. 1 Variations in **a** linear shrinkage and **b** porosity of the scaffolds containing 3 wt% single or composite additives with sintering temperatures

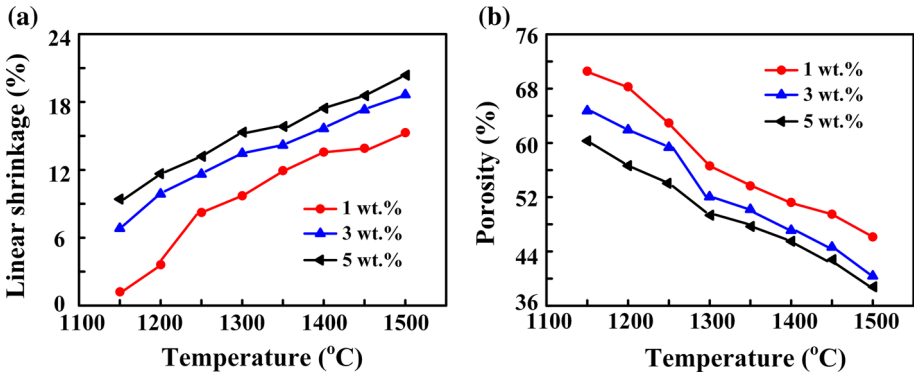

Fig. 2 Variations in **a** linear shrinkage and **b** porosity of the scaffolds containing different amounts of $CuO–TiO_2$ (C/T = 1:2) with sintering temperatures

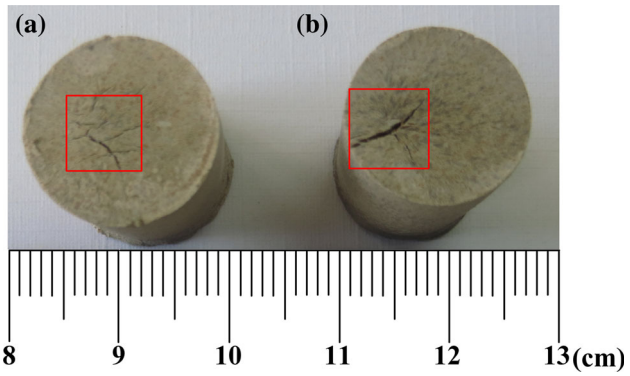

Fig. 3 Photographs of surface cracks in the scaffolds with 5 wt% $CuO–TiO_2$ (C/T = 1:2) after sintering at **a** 1350 °C and **b** 1400 °C

in the scaffold became smaller with the decrease in the C/T ratio. When the C/T ratio was 1:2, part of the Al_2O_3 particles adhered to each other by virtue of a liquid phase, resulting in a noticeable reduction in the lamellar thickness. In the scaffold with the single TiO_2 additive, the Al_2O_3 particles showed apparent agglomeration and growth tendency. Comparing Fig. 5a–d, we can infer that the $CuO–TiO_2$ composite additive, especially when the C/T ratio is 1:2, is more effective in promoting the sinterability of Al_2O_3 than the respective single additive.

Figure 6a–c shows the cross-section microstructures of the scaffolds with different amounts of the $CuO–TiO_2$ additives (C/T = 1:2) sintered at 1300 °C and Fig. 6d gives the statistical results of the corresponding wavelength (λ) and lamellar thickness (d). As indicated, both the wavelength and lamellar thickness decreased with the increase in the amount of the sintering aid, and the lamellar spacing, as calculated from "λ−d", showed a more remarkable reduction. From the inserted high-magnification images, we can see that the Al_2O_3 particles were relatively small and most of them were separately stacked when the amount of the sintering aid was 1 wt%. Increasing sintering aid made the particles closer in arrangement and their sizes larger, indicating enhanced grain growth and adhesion between the particles. Clearly, some Al_2O_3 particles in the scaffold with 5 wt% $CuO–TiO_2$ additive grew into an abnormal morphology.

3.3 Compressive property

Compressive strength is the most important parameter for the characterization of mechanical property of porous scaffolds. Figure 7a shows the variations in the compressive strength with sintering temperature for the scaffolds containing different amounts of $CuO–TiO_2$. In the case of 1 wt% $CuO–TiO_2$, the compressive strength increased from 5 ± 1 MPa for the scaffolds sintered at 1150 °C to 170 ± 25 MPa for those sintered at 1500 °C, while the porosity decreased from 71 to 47 % (Fig. 2b). A significant increase appeared at temperatures between 1350 and 1400 °C (from 52 ± 4 to 103 ± 10 MPa). In the case of 3 wt% $CuO–TiO_2$, the compressive strength increased from 28 ± 3 MPa for the scaffolds sintered at 1150 °C, reaching a maximum value of 176 ± 20 MPa for those sintered at 1450 °C, and then decreased to 125 ± 10 MPa with further increasing the sintering temperature to 1500 °C. The compressive strength of the scaffolds with 5 wt% sintering aid was even larger than that of 1 and 3 wt% when the sintering temperature was no more than 1300 °C. Nevertheless, with the further increase in the sintering temperature, the strength of the scaffolds showed a noticeable decrease. Macrostructural observations (Fig. 3) showed that after high-temperature sintering many cracks appeared in the ceramic walls due to the abnormal grain growth of the Al_2O_3 particles, which should be responsible for the remarkable decrease in the compressive strength. Figure 7b shows the comparison of the maximum compressive strength achieved by directional freeze casting as a function of porosity from the literature data with that of the present work, which was taken from the scaffolds with 3 wt% $CuO–TiO_2$ (C/T = 1:2) and sintered at 1300–1500 °C. The data in literature vary greatly. However, the smaller the porosity, the higher the compression strength. Also, note that the value of 196 MPa with 45 %

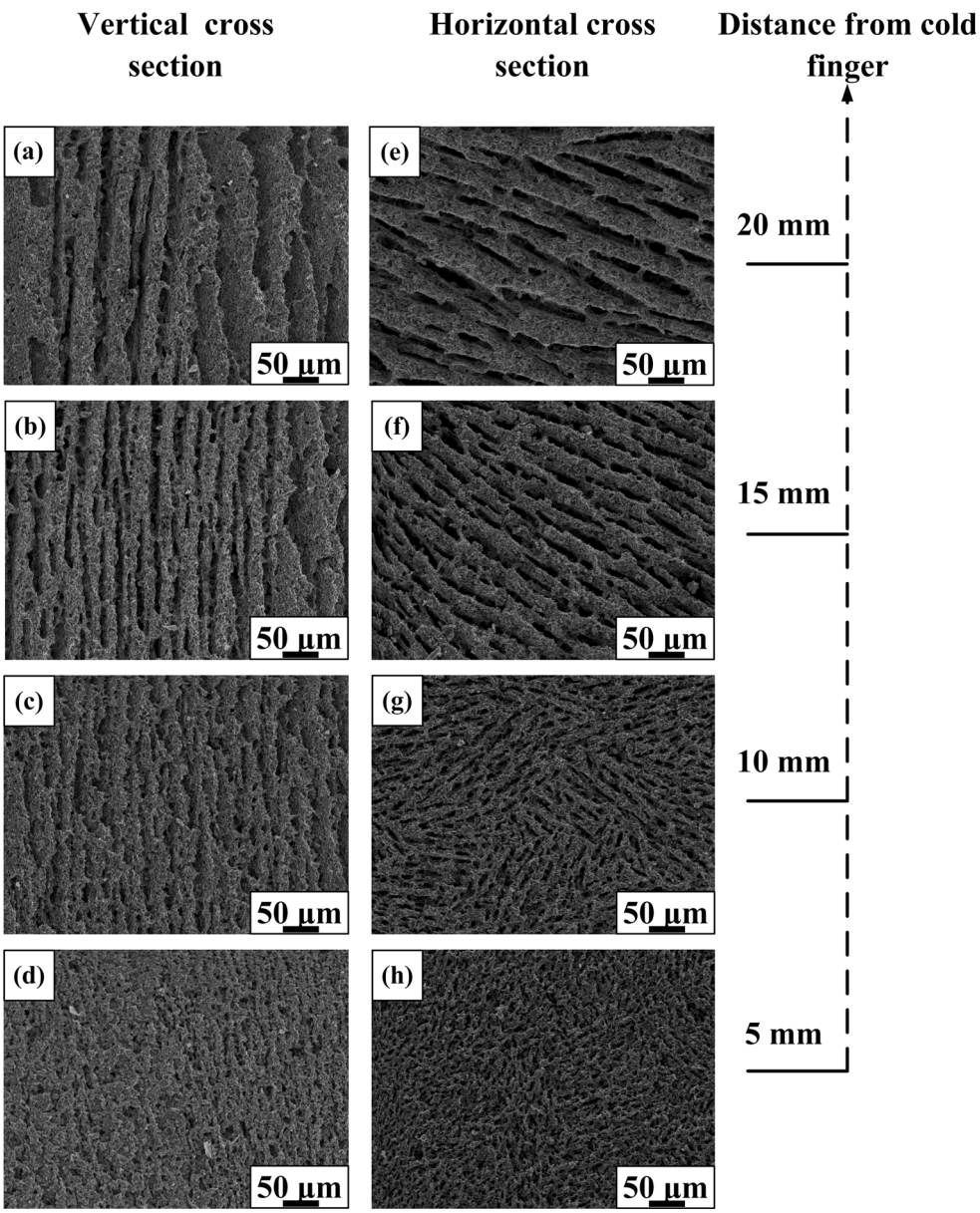

Fig. 4 Microstructures of the Al_2O_3 scaffolds with 3 wt% CuO–TiO_2 (C/T = 1:2) sintered at 1300 °C for 2 h: **a–d** parallel to freezing direction; **e–h** perpendicular to freezing direction

porosity obtained in this work is much higher than the values reported in literature, suggesting a prominent strengthening effect of the CuO–TiO_2 sintering aid.

According to the above analysis, the optimum amount of CuO–TiO_2 sintering aid will be 3 wt% with a mass ratio of 1:2 and the desirable sintering temperature is between 1300 and 1450 °C.

4 Discussion

The above results showed that CuO–TiO_2 sintering aids could greatly promote the sinterability of Al_2O_3, leading to a substantial improvement in compressive strength of the scaffolds. However, the sinter-aiding mechanism was still unclear and worthy of discussion here. We suggest the following possibilities:

1. Formation of Cu–Al–O liquid phase

According to CuO–Al_2O_3 phase diagram (Fig. 8a), CuO would transform to Cu_2O at about 1000 °C and then form a eutectic liquid by reaction with Al_2O_3 (more exactly with $CuAlO_2$) at about 1130 °C [24]. The presence of this liquid phase would not only rearrange the particles but also enhance the mass transfer, and thus promote the densification of Al_2O_3. But this effect is not very significant, especially at temperatures lower than 1400 °C, as seen from Figs. 1 and 5a.

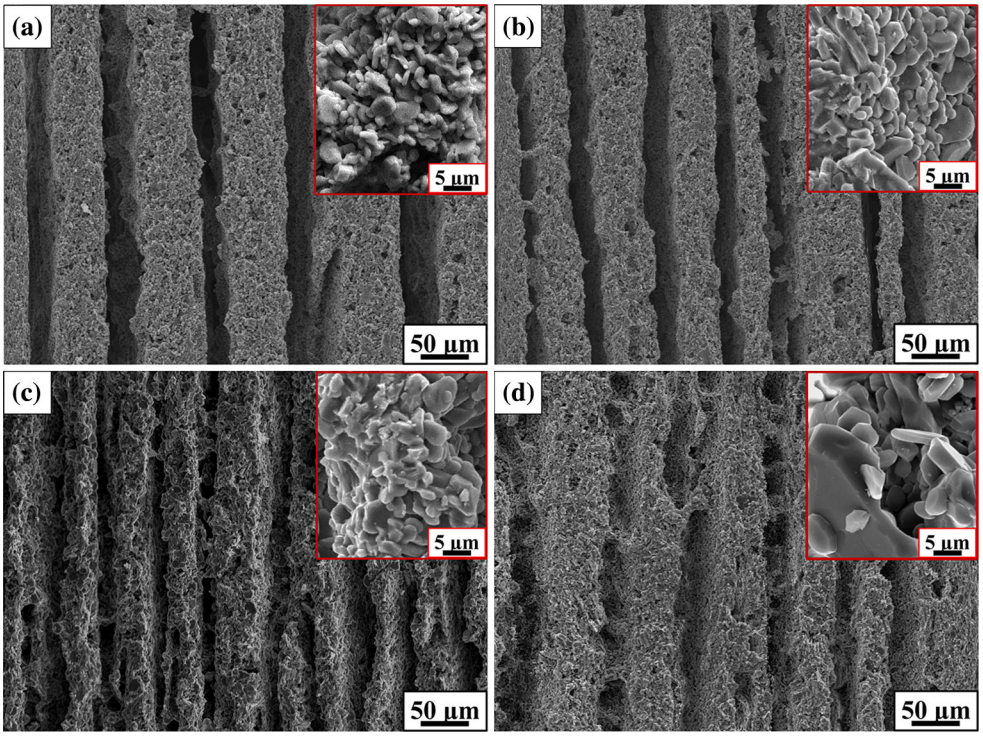

Fig. 5 SEM micrographs of the scaffolds with 3 wt% single or composite additives sintered at 1300 °C for 2 h: **a** CuO; **b** C/T = 5:1; **c** C/T = 1:2; **d** TiO_2

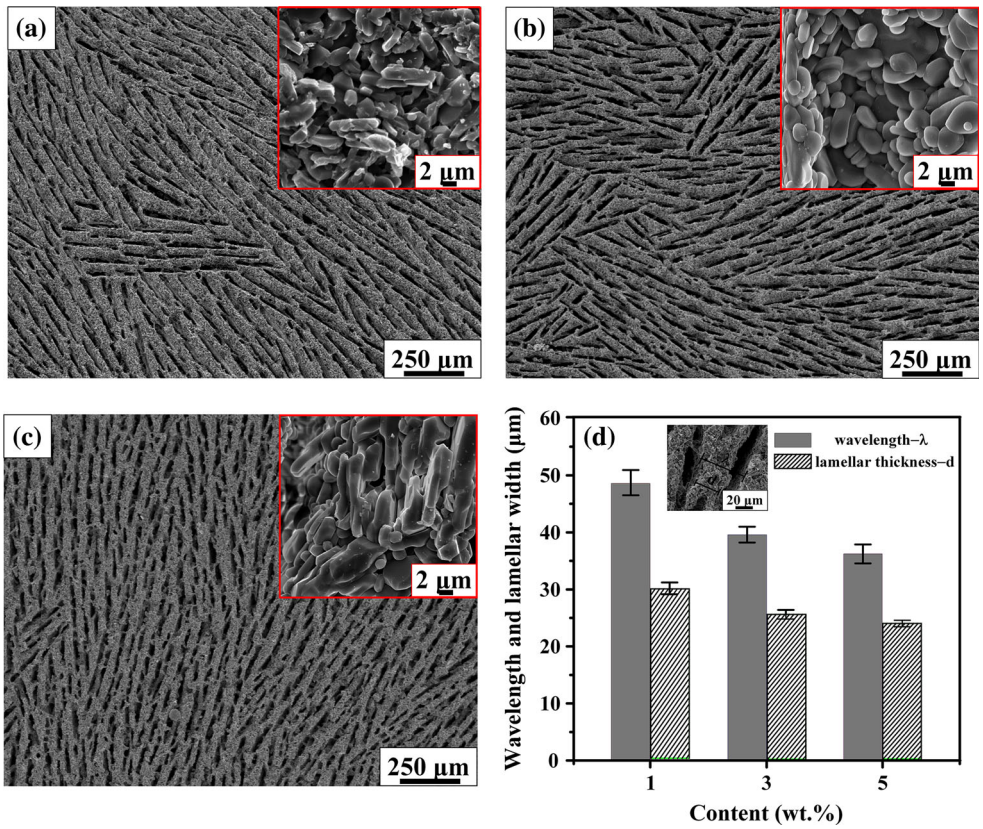

Fig. 6 Cross-section microstructures of the scaffolds with different amounts of CuO–TiO_2 (C/T = 1:2) after sintering at 1300 °C for 2 h: **a** 1 wt%, **b** 3 wt% and **c** 5 wt%; **d** Variation in wavelength (λ) and lamellar thickness (*d*) with the amount of CuO–TiO_2 (C/T = 1:2)

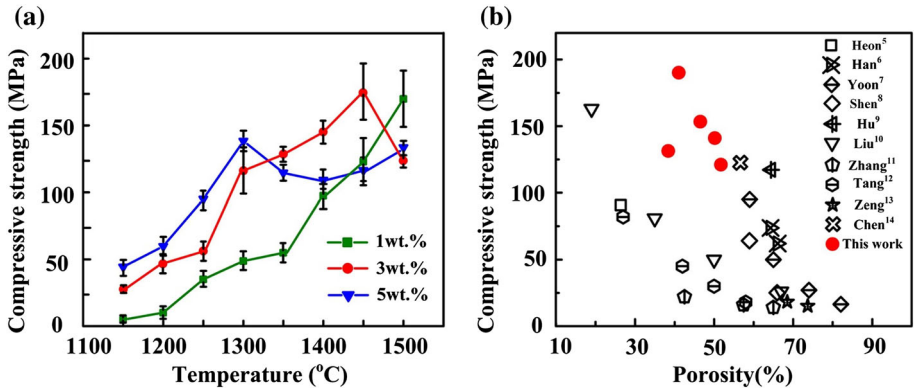

Fig. 7 **a** Variation in compressive strength with sintering temperature for the scaffolds containing different amounts of $CuO–TiO_2$ (C/T = 1:2). **b** Comparison of the maximum compressive strength achieved by directional freeze casting as a function of porosity from literature data and the present work

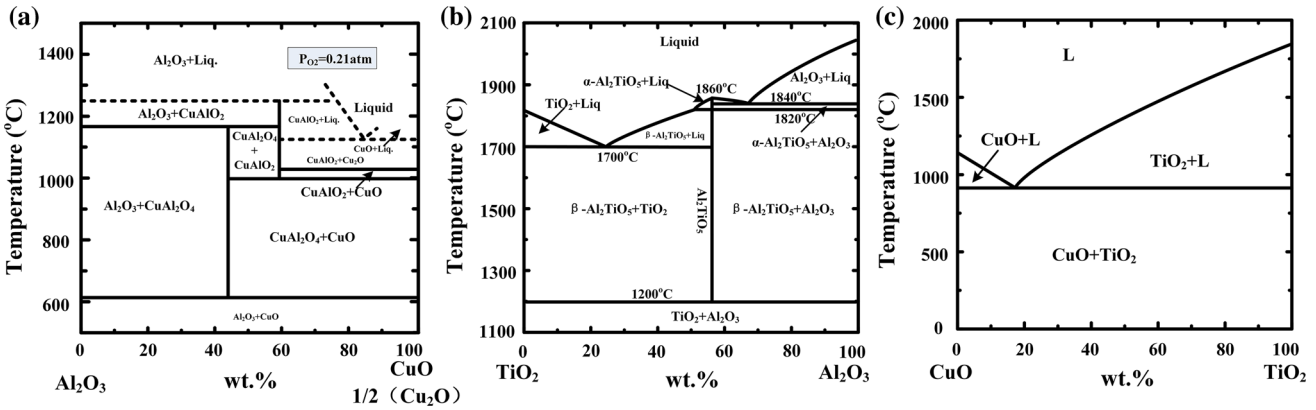

Fig. 8 Phase diagrams of **a** $CuO–Al_2O_3$ [24], **b** $TiO_2–Al_2O_3$ [25], and **c** $CuO–TiO_2$ [27]

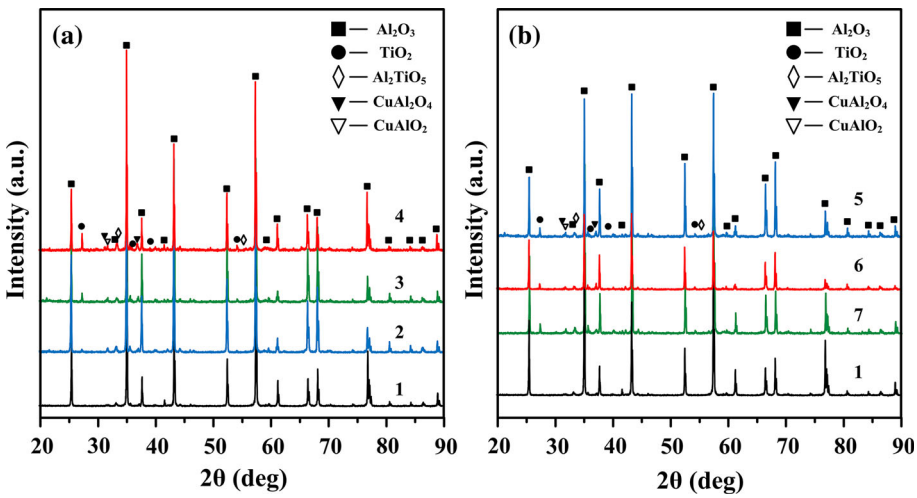

Fig. 9 XRD patterns for **a** the scaffolds sintered at 1300 °C with different amounts of $CuO–TiO_2$ (C/T = 1:2): *1* 0 wt% (i.e., raw Al_2O_3 powders); *2* 1 wt%; *3* 3 wt% and *4* 5 wt%, and **b** the scaffolds with 3 wt% $CuO–TiO_2$ (C/T = 1:2) sintered at different temperatures: *5* 1300 °C; *6* 1400 °C and *7* 1500 °C

2. Formation of limited substitution solid solution

As indicated in Fig. 9, several weak peaks corresponding to TiO_2, Al_2TiO_5, $CuAl_2O_4$ and $CuAlO_2$ were identified, particularly for the samples with the addition of a relatively large amount of sintering aids or sintered at higher temperatures. The presence of Al_2TiO_5, $CuAl_2O_4$ and $CuAlO_2$ is generally consistent with the respective phase diagrams (Fig. 8). From the $TiO_2–Al_2O_3$ phase diagram (Fig. 8b), when the temperature is above 1200 °C, TiO_2 can react with Al_2O_3 to form Al_2TiO_5, lowering the sintering activation energy of Al_2O_3. From the crystallographic point of view, TiO_2 has very similar lattice

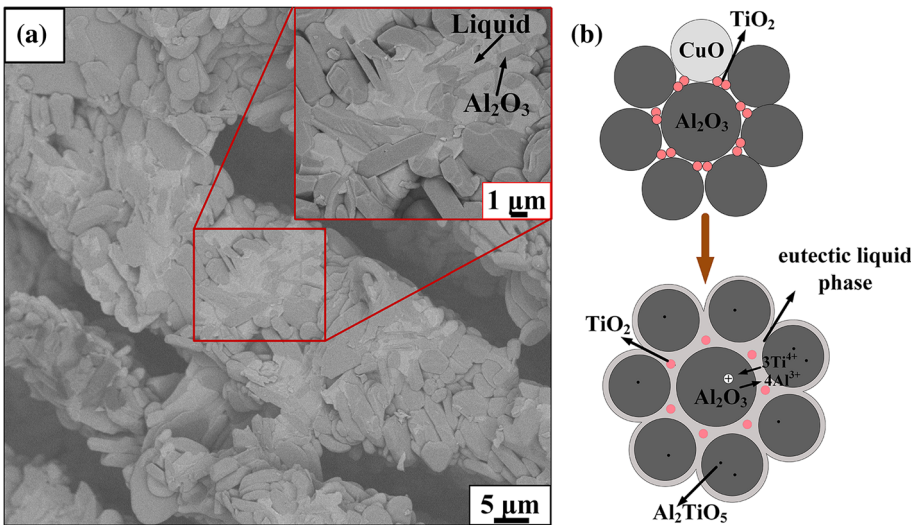

Fig. 10 **a** Backscattered electron image of the Al_2O_3 particles surrounded by an irregular-shaped liquid phase from the scaffold containing 3 wt% CuO–TiO_2 (C/T = 1:2) sintered at 1400 °C. **b** Schematic diagram for illustration of the formation of CuO–TiO_2 eutectic in promoting the sintering of Al_2O_3

constants with Al_2O_3, and therefore it could interact with Al_2O_3 to form limited substitutional solid solution [25] during the sintering process, which enhanced atomic diffusion and promoted sintering by increasing the lattice defect populations. Moreover, in order to maintain electrical neutrality, three Ti^{4+} replaced out of four Al^{3+} and left a positive ion vacancy, resulting in an increase in vacancy concentration and diffusion coefficient. The formation of vacancy and lattice distortion could lead to the recrystallization and densification of Al_2O_3 in an effective way [26]. On the other hand, the presence of residual TiO_2 in the scaffolds with 5 wt% sintering aid suggests an excessive addition of this phase, which led to the abnormal grain growth of the alumina particles.

3. Formation of CuO–TiO_2 eutectic melt

Figure 10a shows the back-scattered electron image of the Al_2O_3 particles surrounded by an irregular-shaped phase, which was presumed to be the eutectic phase. Figure 10b shows a schematic diagram for illustrating the formation of CuO–TiO_2 eutectic and its role in promoting the sintering. As shown in CuO–TiO_2 phase diagram (Fig. 8c), a eutectic phase forms at about 920 °C [27], which is much lower than the eutectic point of Cu–Al–O (1130 °C [24]). Hence, a CuO–TiO_2 liquid phase would first appear if the particles could intimately contact with each other. The co-existance of TiO_2 and CuO was presumed to increase the solubility of each other due to mutual charge compensation [28]. Moreover, the TiO_2 powders used in this experiment were nanoparticles with high surface activity and larger solubility in a liquid phase than in the solid Al_2O_3 crystal. Because of the presence of liquid, the solution temperature of TiO_2 was significantly reduced. Therefore, with the increase in the solubility of Ti^{4+}, the exchange between Al^{3+} and Ti^{4+} was greatly accelerated, which in turn increased the ion vacancy concentration and atomic diffusion coefficient. Owing to these effects, the sintering of the Al_2O_3 scaffolds was greatly promoted and the compressive strength increased.

5 Conclusions

1. Porous Al_2O_3 scaffolds with high compressive strength (97–197 MPa) and relatively large porosity (51–45 %) can be obtained by freeze casting of the alumina suspensions with 3 wt% CuO–TiO_2 additive in a mass ratio of 1:2 in the slurries and then sintering of the green bodies between 1300 and 1450 °C.
2. The introduction of CuO–TiO_2 sintering aid significantly reduces the sintering temperature, promotes the densification and increases the strength of porous Al_2O_3 scaffolds. The sinter-aiding mechanism of the CuO–TiO_2 additive is mainly ascribed to the formation of limited substitutional solution and a eutectic phase, thus increasing ion vacancy concentration and atomic diffusion. Nevertheless, an excessive addition and a higher sintering temperature could give rise to cracks in the sintered scaffolds.

Acknowledgments This work is supported by National Natural Science Foundation of China (No. 51571099), National Basic Research Program of China (973 program) (No. 2012CB619600) and the Fundamental Research Funds for the Central Universities (Jilin University).

References

1. S. Deville, E. Saiz, A.P. Tomsia, Biomaterials **27**, 5480 (2006)
2. S. Deville, E. Saiz, R.K. Nalla, A.P. Tomsia, Science **311**, 515 (2006)

3. S. Deville, E. Saiz, A.P. Tomsia, Acta Mater. **55**, 1965 (2007)
4. S. Deville, Adv. Eng. Mater. **10**, 155 (2008)
5. K.K. Heon, K.T. Rim, K.D. Hyun, J. Korean Ceram. Soc. **51**, 19 (2014)
6. J.C. Han, L.Y. Hu, Y.M. Zhang, J. Am. Ceram. Soc. **92**, 2165 (2009)
7. B.H. Yoon, W.Y. Choi, H.E. Kim, J.H. Kim, Y.H. Koh, Scr. Mater. **58**, 537 (2008)
8. P. Shen, J.W. Xi, Y.J. Fu, A. Shaga, C. Sun, Q.C. Jiang, Acta Metall. Sin. **27**, 944 (2014)
9. L.Y. Hu, Y.M. Zhang, S.L. Dong, S.M. Zhang, B.X. Li, Ceram. Int. **39**, 6287 (2013)
10. G. Liu, D. Zhang, C. Meggs, T.W. Button, Scr. Mater. **62**, 466 (2010)
11. D. Zhang, Y. Zhang, R. Xie, K.C. Zhou, Ceram. Int. **38**, 6063 (2012)
12. Y.F. Tang, Q. Miao, S. Qiu, K. Zhao, L. Hu, J. Eur. Ceram. Soc. **34**, 4077 (2014)
13. J. Zeng, Y. Zhang, K. Zhou, D. Zhang, Trans. Nonferr. Metal Soc. **24**, 718 (2014)
14. R.F. Chen, C.A. Wang, Y. Huang, L.G. Ma, W.Y. Lin, J. Am. Ceram. Soc. **90**, 3478 (2007)
15. C.Q. Hong, X.H. Zhang, J.C. Han, J.C. Du, W.B. Han, Scr. Mater. **60**, 563 (2009)
16. J. Tang, Y.F. Chen, H. Wang, Key Eng. Mater. **280**, 1287 (2004)
17. F. Ye, J. Zhang, H. Zhang, Mater. Sci. Eng. A **527**, 6501 (2010)
18. M.M. Porter, R. Imperio, M. Wen, Adv. Funct. Mater. **24**, 1978 (2014)
19. W.J. Smothers, H.J. Reynolds, J. Am. Ceram. Soc. **37**, 588 (1954)
20. D.S. Horn, G.L. Messing, Mater. Sci. Eng. A **195**, 169 (1995)
21. C.G. Li, Academic Annual Meeting of the Chinese Society of Silicate, Beijing, p. 25 (2003)
22. M. Sathiyakumar, F.D. Gnanam, J. Mater. Process. Technol. **133**, 282 (2003)
23. U.G.K. Wegst, M. Schecter, A.E. Donius, P.M. Hunger, Philos. Trans. R. Soc. A **368**, 2099 (2010)
24. A.M.M. Gadalla, J. White, J. Br. Ceram. Soc. **63**, 39 (1964)
25. L.Z. Huang, J.X. Zhang, Ordnance. Mater. Sci. Eng. **5**, 3 (1998)
26. D.R. Clarke, T.M. Shaw, D. Dimos, J. Am. Ceram. Soc. **72**, 1103 (1989)
27. F.H. Lu, F.X. Fang, Y.S. Chen, J. Eur. Ceram. Soc. **21**, 1093 (2001)
28. L.A. Xue, I.W. Chen, J. Am. Ceram. Soc. **74**, 2011 (1991)